Electronic Supporting Information

Surface-Enhanced Raman Scattering from Au Nanorods, Nanotriangles, and Nanostars with Tuned Plasmon Resonances

Boris N. Khlebtsov,[a] *Andrey M. Burov,*[a] *Sergey V. Zarkov,*[a] *Nikolai G. Khlebtsov,*[a,b,*]

[a]Institute of Biochemistry and Physiology of Plants and Microorganisms, "Saratov Scientific Centre of the Russian Academy of Sciences," 13 Prospekt Entuziastov, Saratov 410049, Russia

[b]Saratov State University, 83 Ulitsa Astrakhanskaya, Saratov 410012, Russia

Corresponding author (NGK): khlebtsov@ibppm.ru

Table of Content

Section S1. Additional data for AuNR, AuNR@NBT, and AuNR@Cy7.5 samples

Section S1.1. Additional TEM images

A

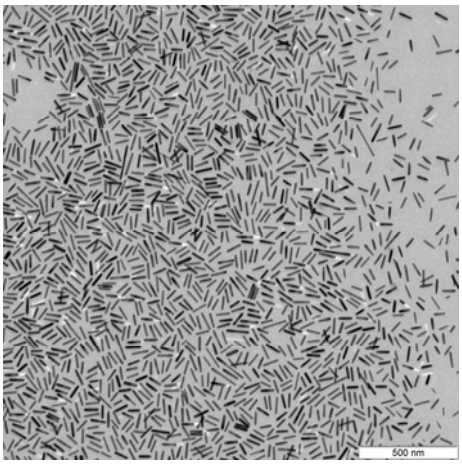

B

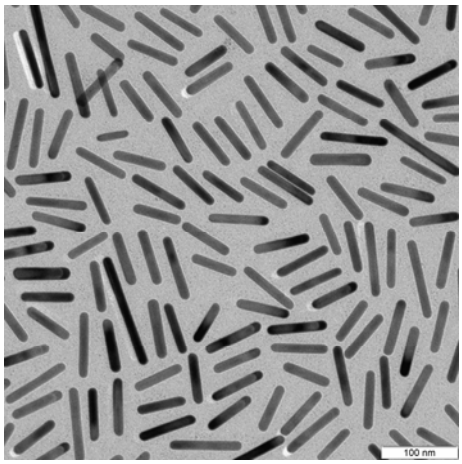

C

D

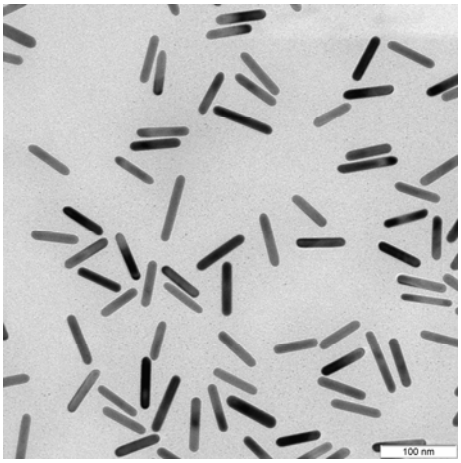

E

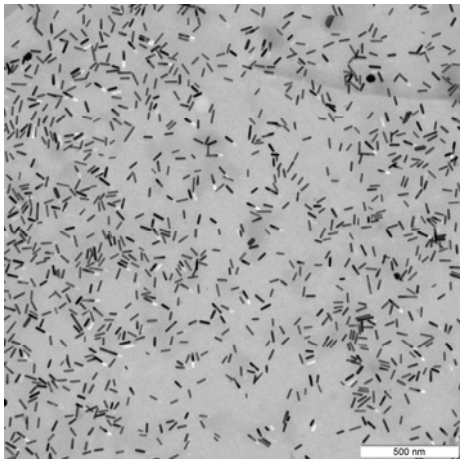

F

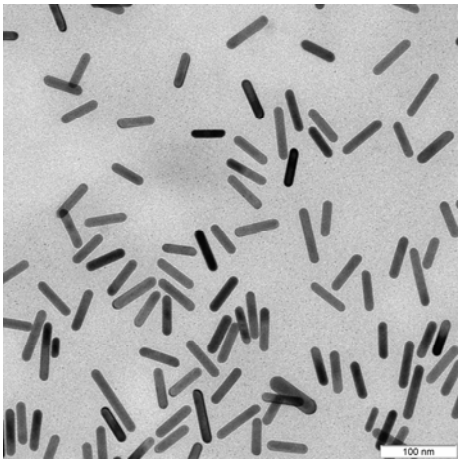

G

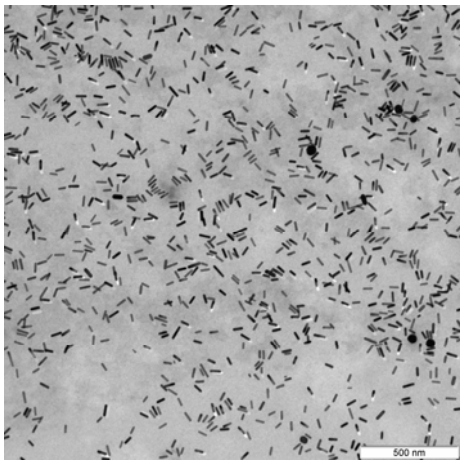

H

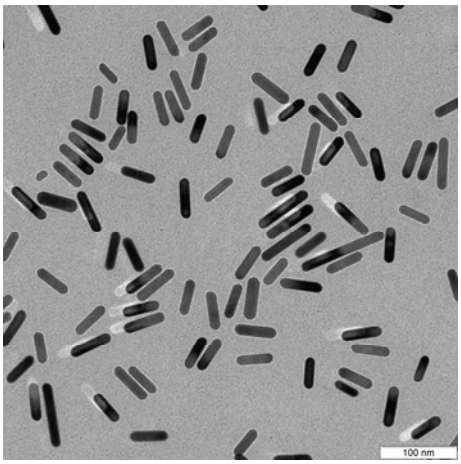

I

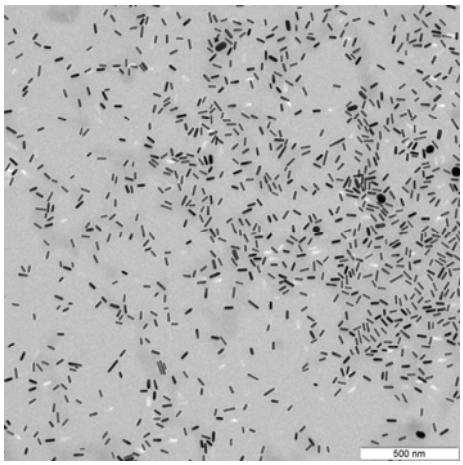

J

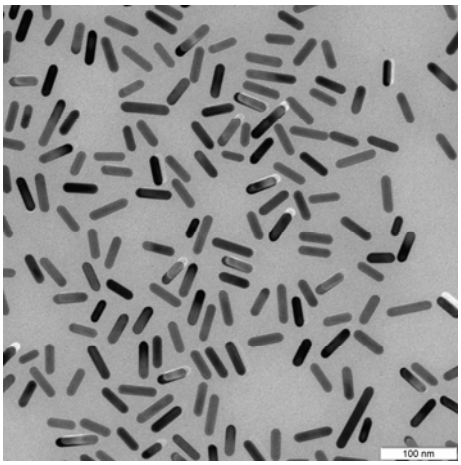

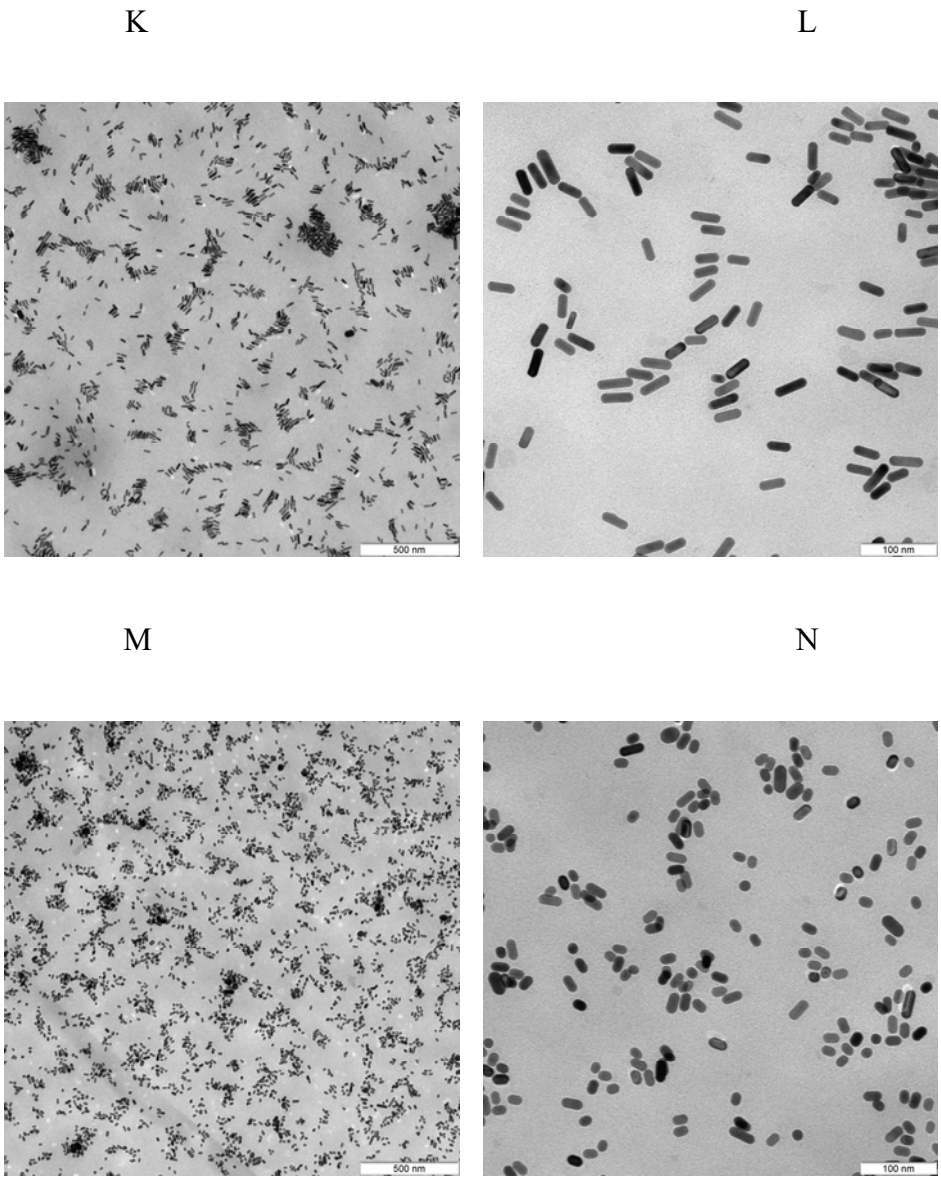

Figure S1. TEM images of samples 1 (A, B), 3 (C, D), 5 (E, F), 7 (G, H), 9 (I, J), 11 (K, L), and 13 (M, N). The scale bars are 500 nm (left column) and 100 nm (right column).

Section S1.2. Histograms of the aspect ratio (AR), length (L), and diameter (D) distributions for AuNR samples 1-12.

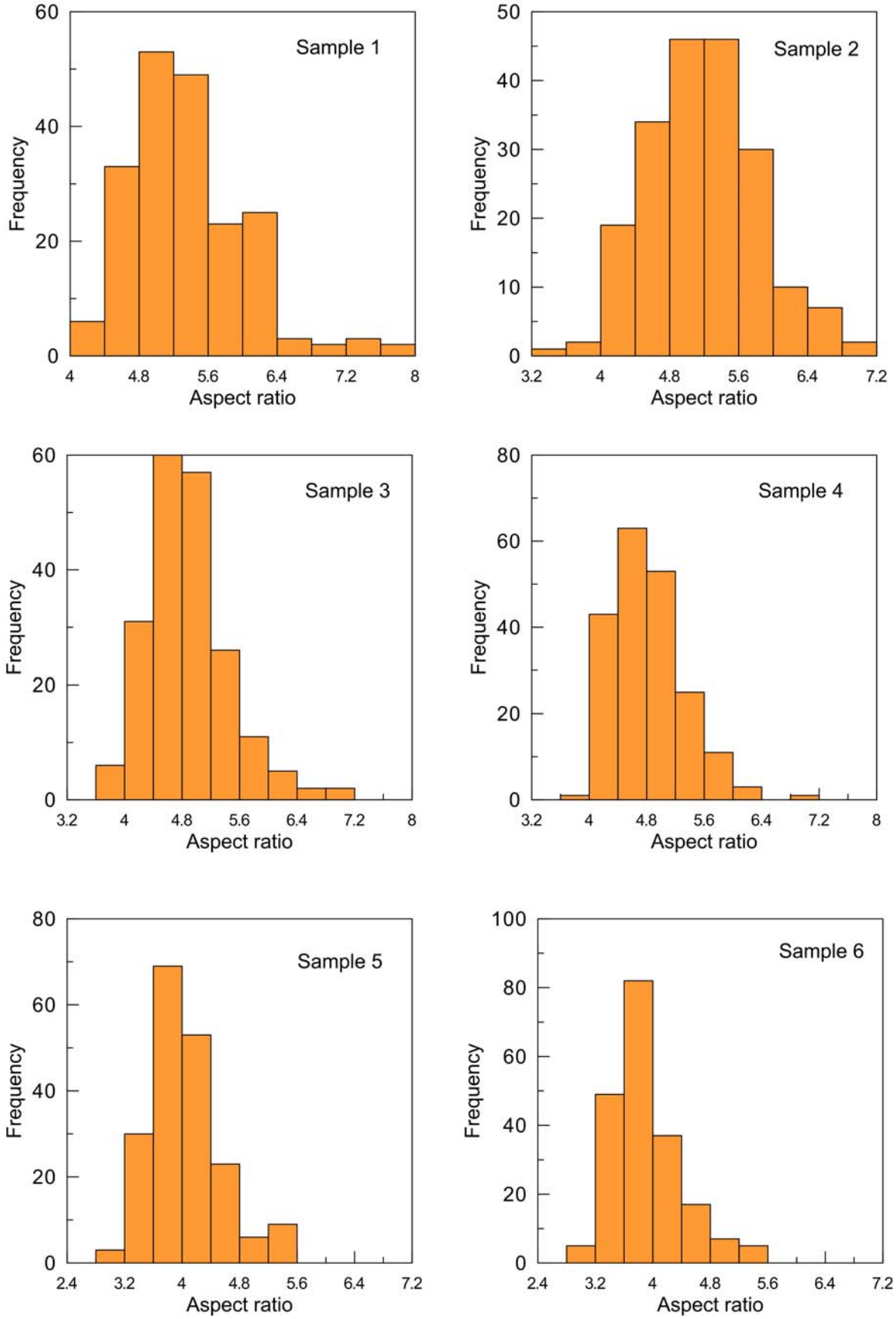

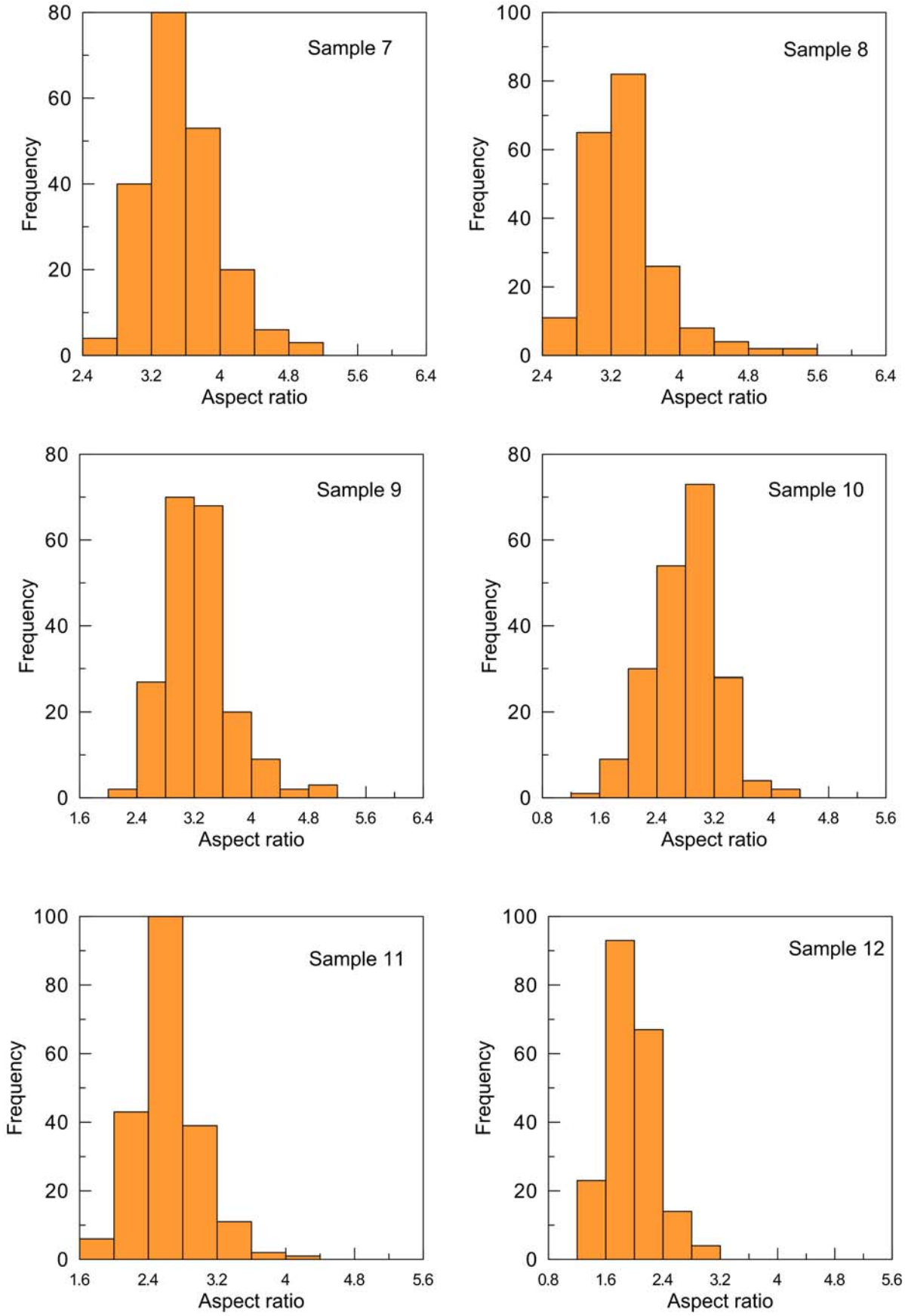

Figure S2. Histograms of the aspect ratio distribution for samples 1-12.

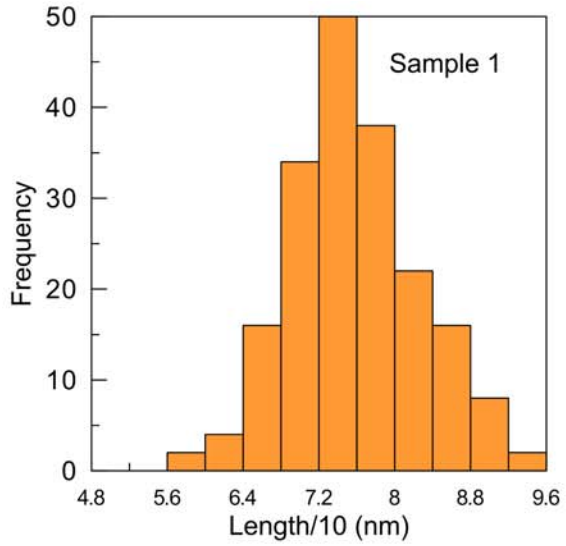
Sample 1
Frequency
Length/10 (nm)
0
10
20
30
40
50
4.8
5.6
6.4
7.2
8
8.8
9.6

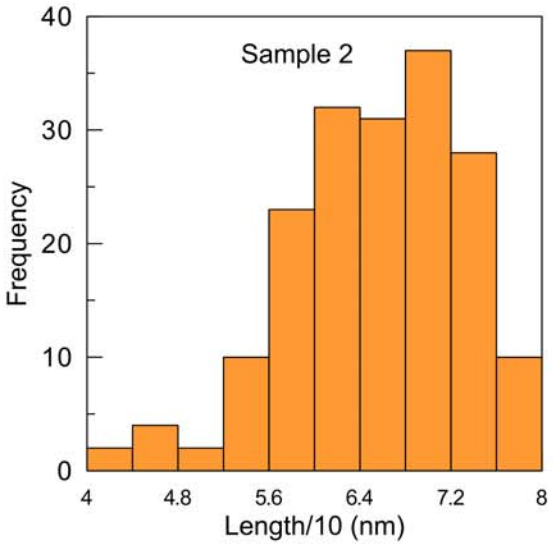
Sample 2
Frequency
Length/10 (nm)
0
10
20
30
40
4
4.8
5.6
6.4
7.2
8

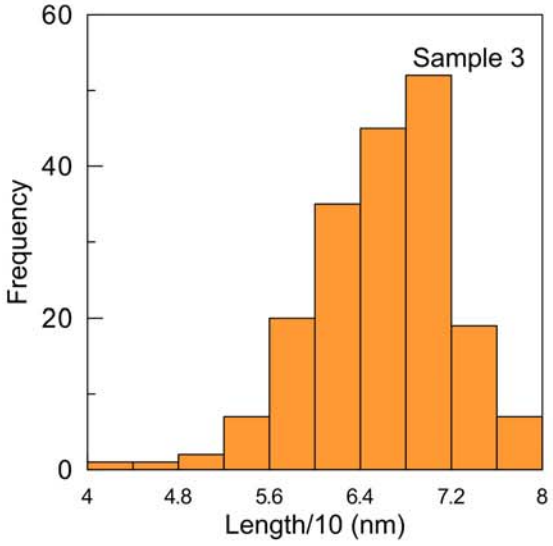
Sample 3
Frequency
Length/10 (nm)
0
20
40
60
4
4.8
5.6
6.4
7.2
8

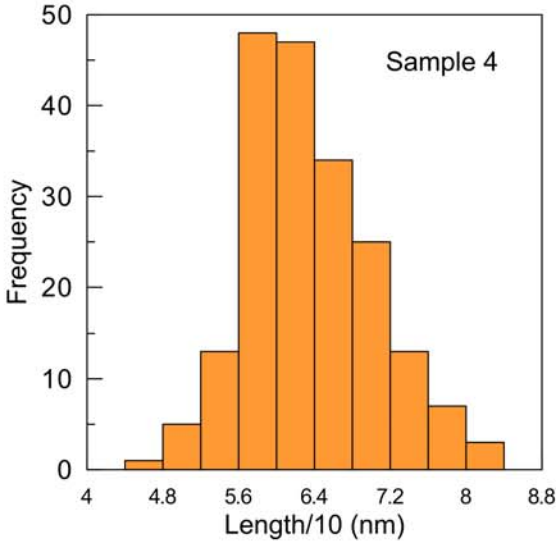
Sample 4
Frequency
Length/10 (nm)
0
10
20
30
40
50
4
4.8
5.6
6.4
7.2
8
8.8

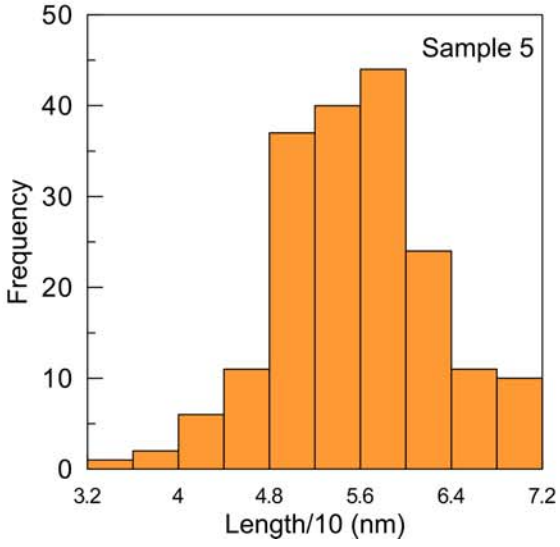
Sample 5
Frequency
Length/10 (nm)
0
10
20
30
40
50
3.2
4
4.8
5.6
6.4
7.2

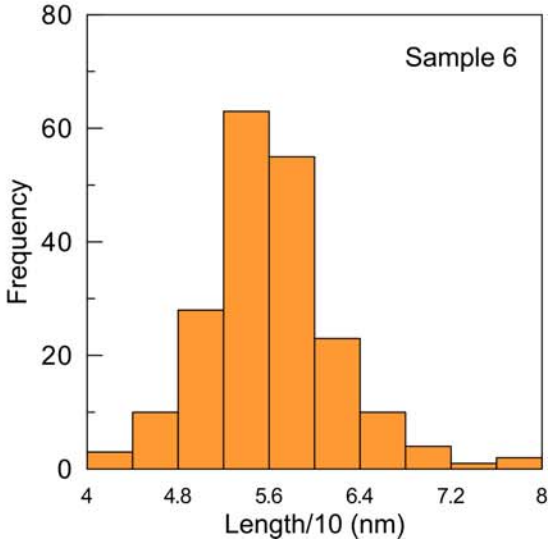
Sample 6
Frequency
Length/10 (nm)
0
20
40
60
80
4
4.8
5.6
6.4
7.2
8

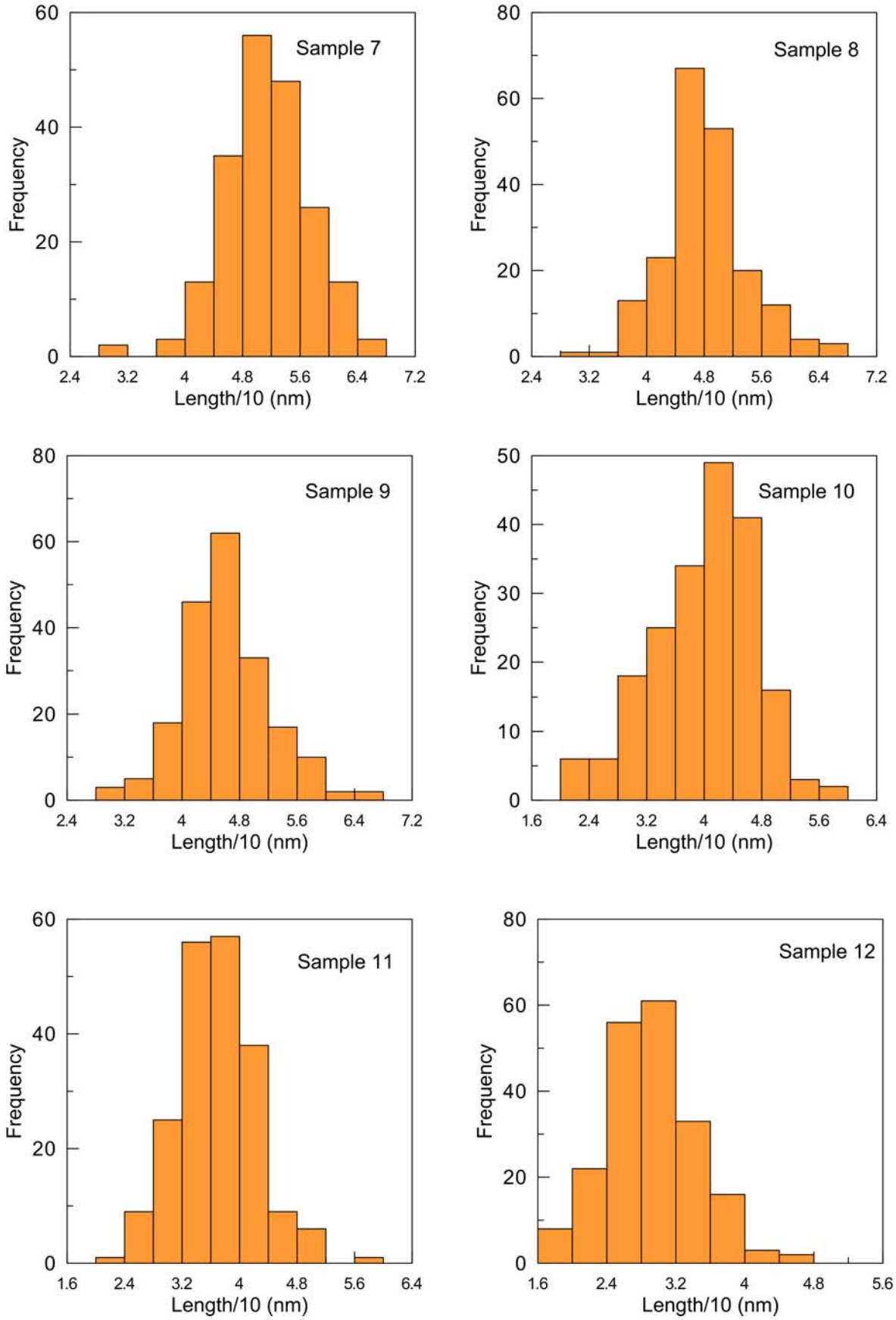

Figure S3. Histograms of the AuNR length distribution for samples 1-12.

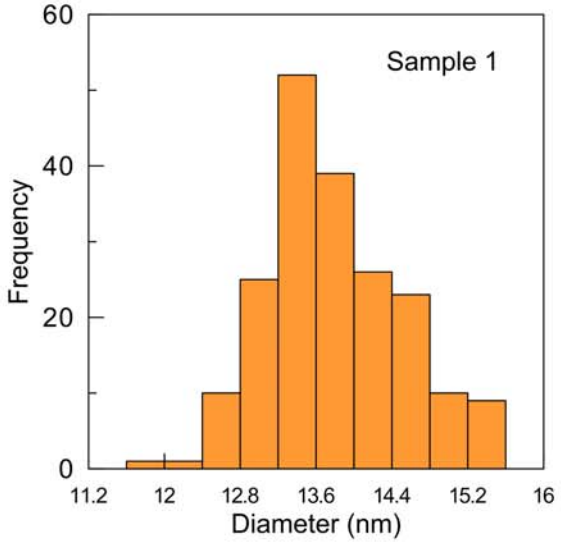
Sample 1
Frequency
Diameter (nm)
0
20
40
60
11.2
12
12.8
13.6
14.4
15.2
16

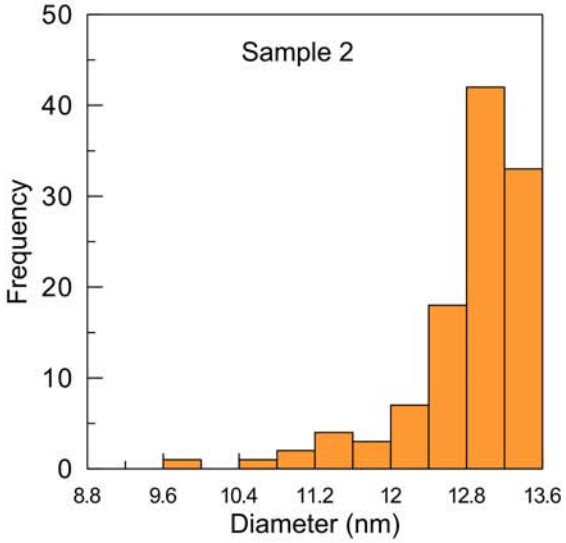
Sample 2
Frequency
Diameter (nm)
0
10
20
30
40
50
8.8
9.6
10.4
11.2
12
12.8
13.6

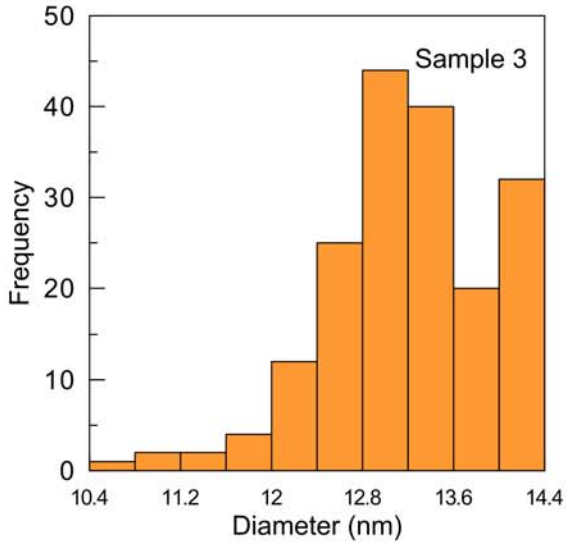
Sample 3
Frequency
Diameter (nm)
0
10
20
30
40
50
10.4
11.2
12
12.8
13.6
14.4

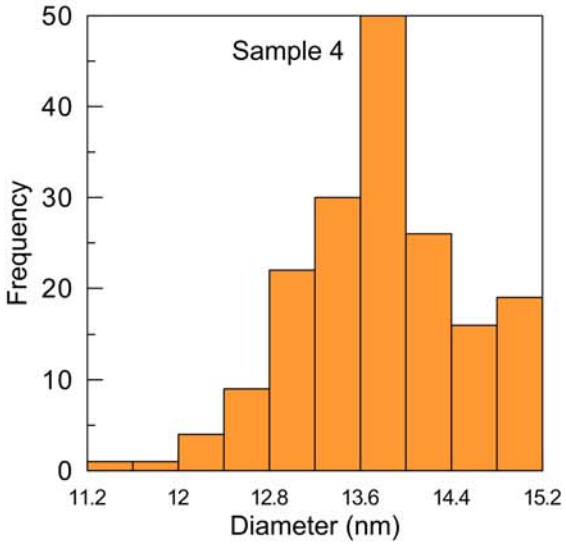
Sample 4
Frequency
Diameter (nm)
0
10
20
30
40
50
11.2
12
12.8
13.6
14.4
15.2

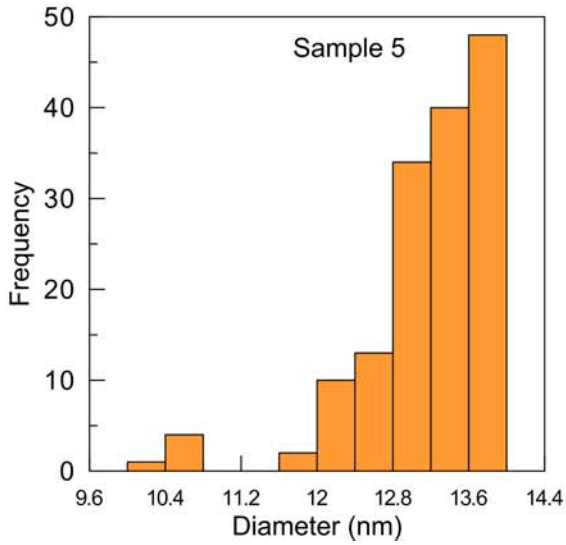
Sample 5
Frequency
Diameter (nm)
0
10
20
30
40
50
9.6
10.4
11.2
12
12.8
13.6
14.4

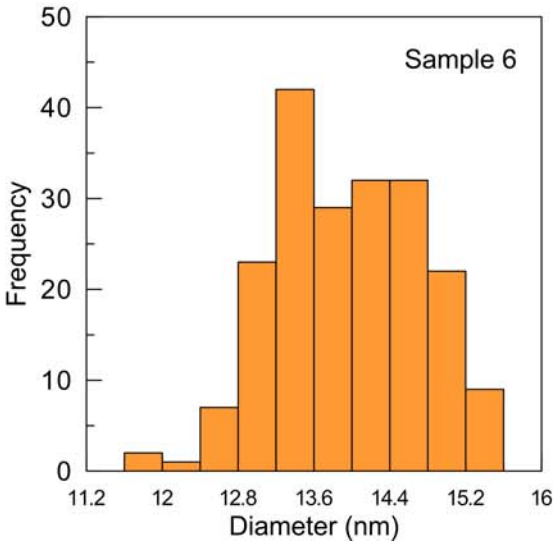
Sample 6
Frequency
Diameter (nm)
0
10
20
30
40
50
11.2
12
12.8
13.6
14.4
15.2
16

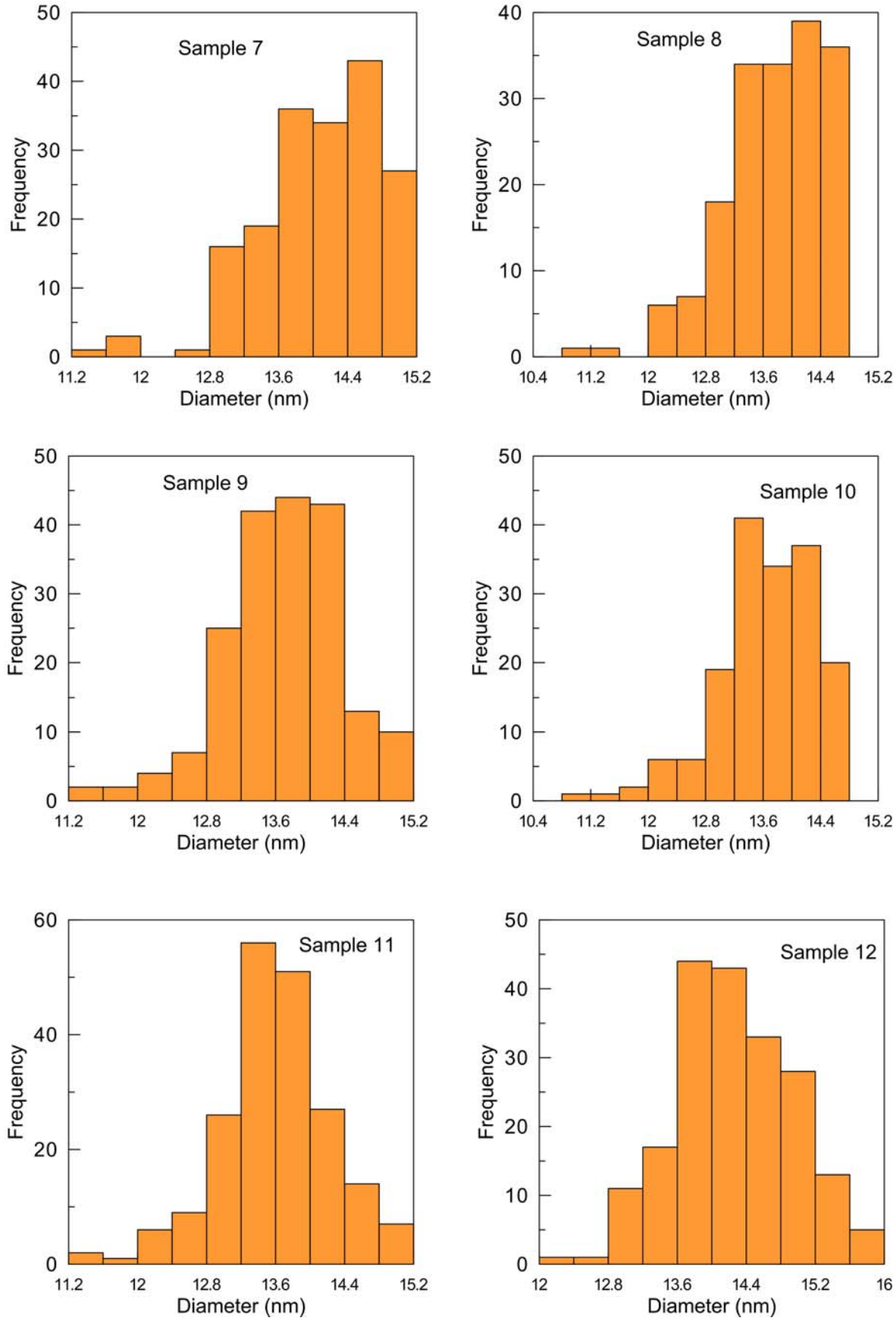

Figure S4. Histograms of the AuNR diameter distribution for samples 1-12.

Section S1.3. T-matrix simulated extinction spectra for polydisperse AuNR ensembles.

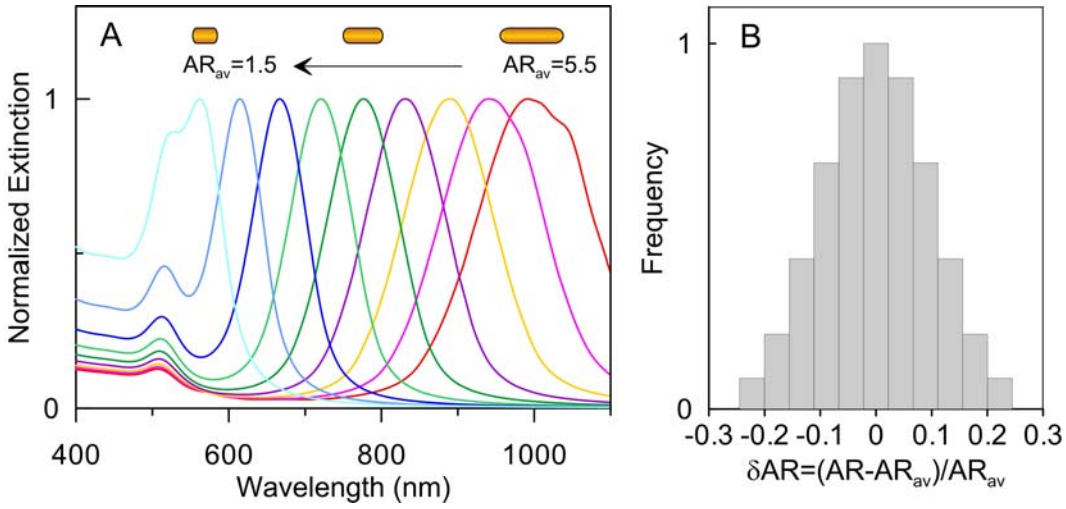

Figure S5. T-matrix simulated extinction spectra for polydisperse randomly oriented AuNRs with the average aspect ratios $AR_{av} = 1.5 - 5.5(0.5)$ (A). Panel B shows the aspect ratio distribution of each ensemble with relative STD =0.1 (in terms of the normalized dispersion of the Gaussian distribution). The constant average diameter equals 13.8 nm for all samples.

Section S1.4 SERS measurements for AuNR@NBT and AuNR@Cy7.5 samples at 785- and 633-nm laser excitation.

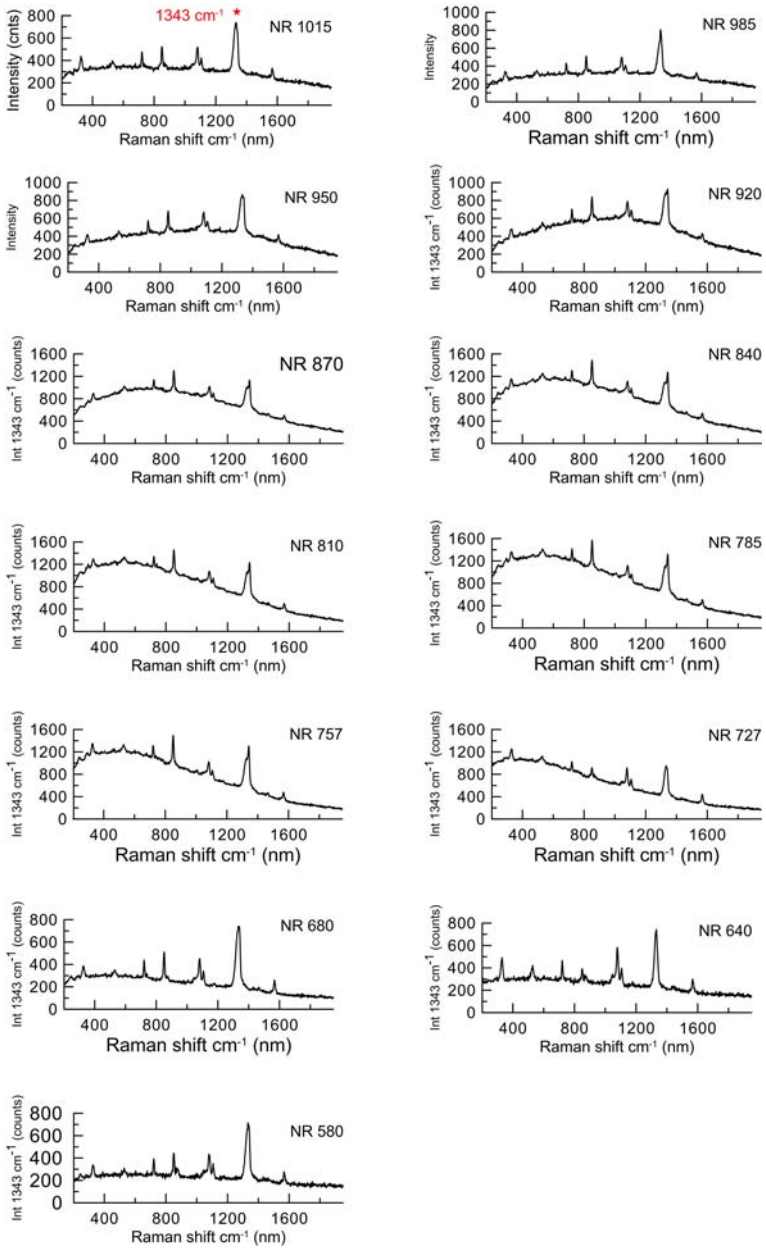

Figure S6. SERS spectra for 13 AuNR@NBT samples measured at 785 nm laser excitation. The LPR wavelengths varied from 1017 to 580 nm.

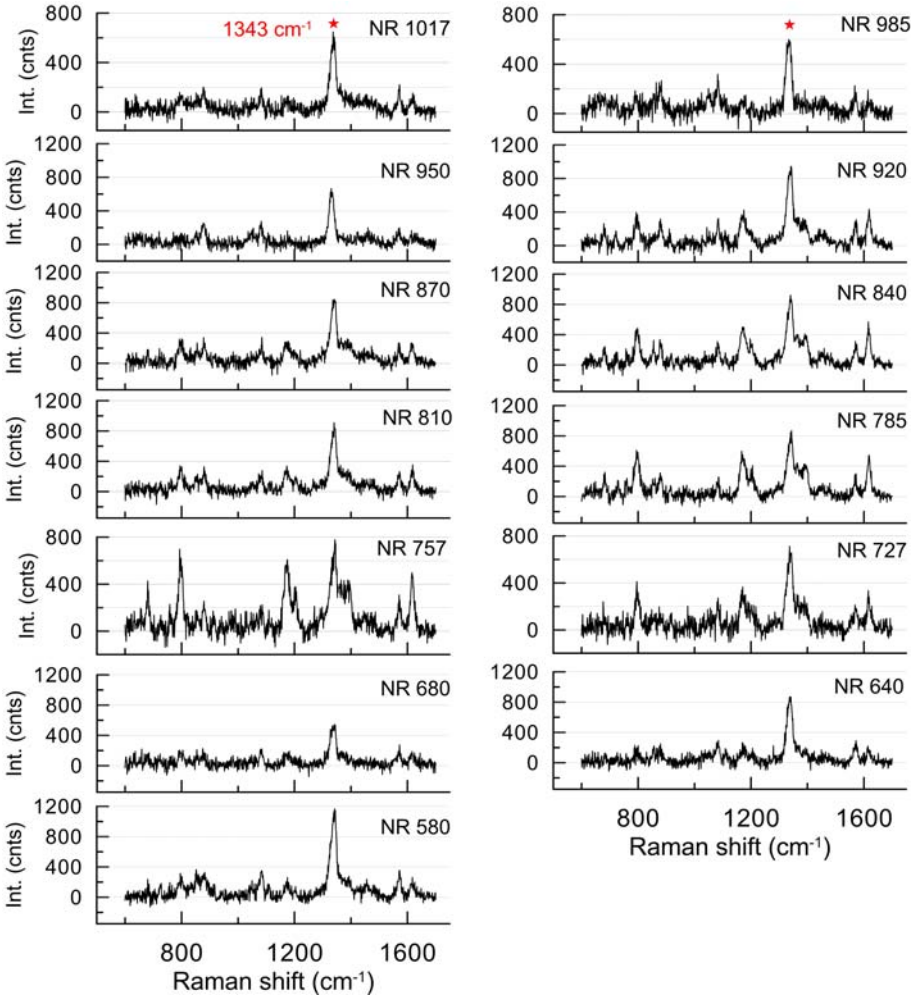

Figure S7. SERS spectra for AuNR@NBT samples measured at 633 nm laser excitation. The LPR wavelengths varied from 1017 to 580 nm.

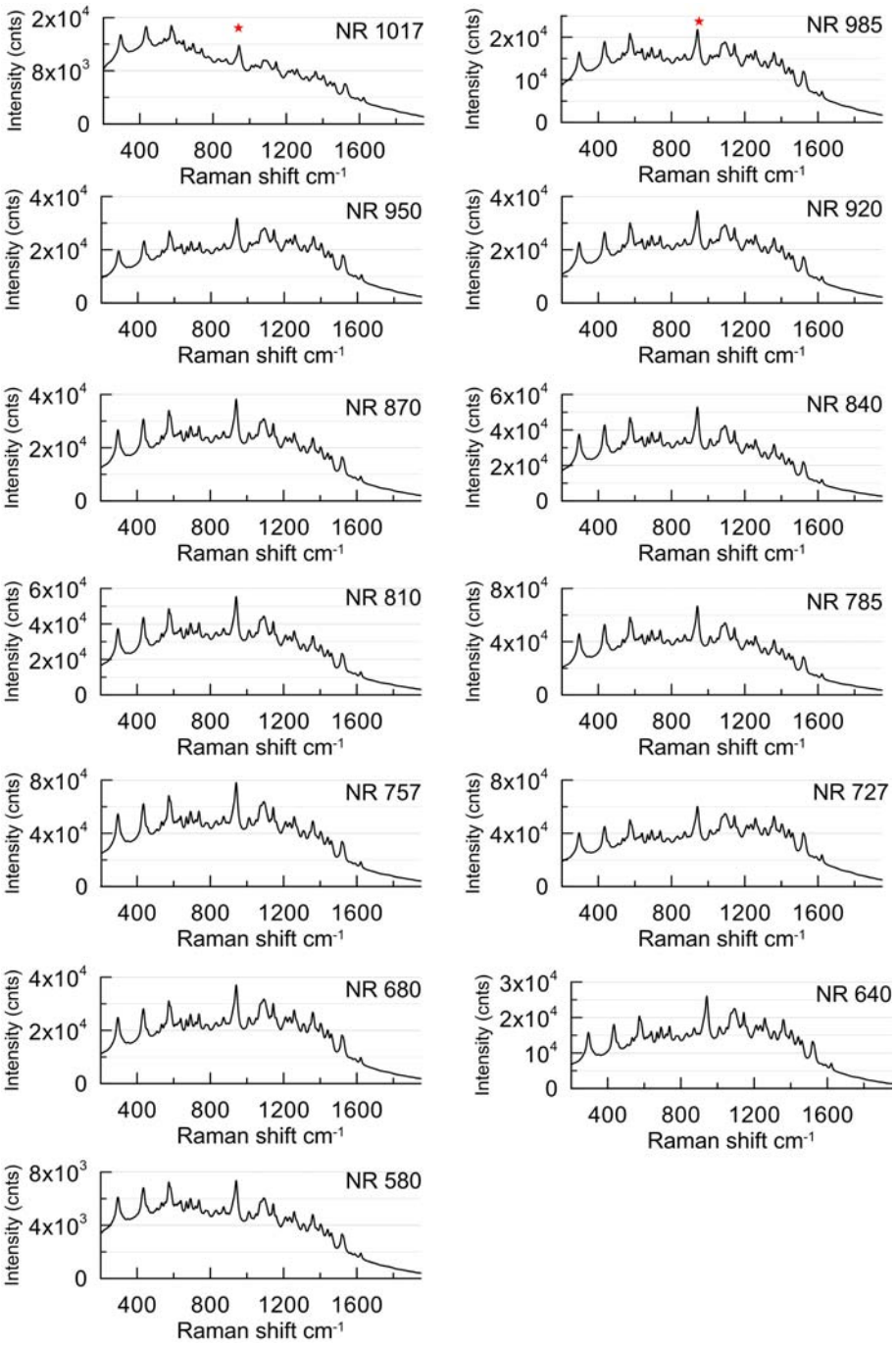

Figure S8. SERS spectra for AuNR@Cy7.5 samples measured at 785 nm laser excitation. The LPR wavelength decreases from 1017 to 580 nm.

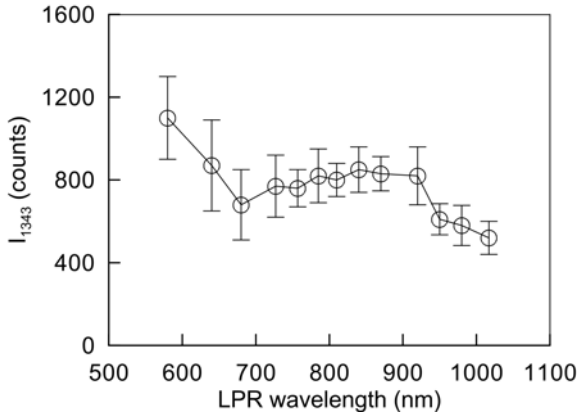

Figure S9. SERS peak intensity I_{1343} of AuNR@NBT conjugates at 633 nm laser excitation as a function of LPR wavelength.

Section S2. Additional data for AuNT, AuNT@NBT,and AuNT@Cy7.5 samples

Section S2.1. Additional TEM images of initial and etched AuNT nanoparticles for samples 1-8

A

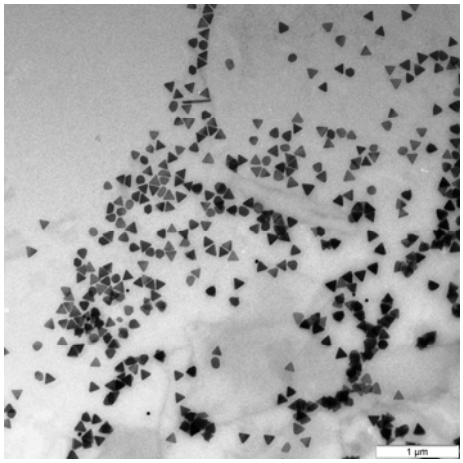

B

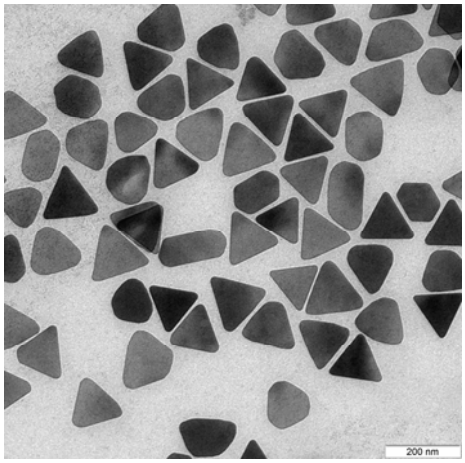

C

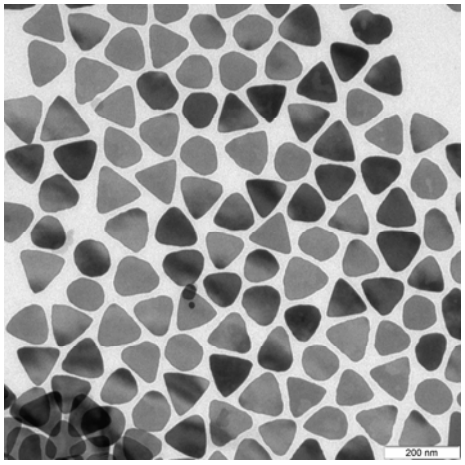

D

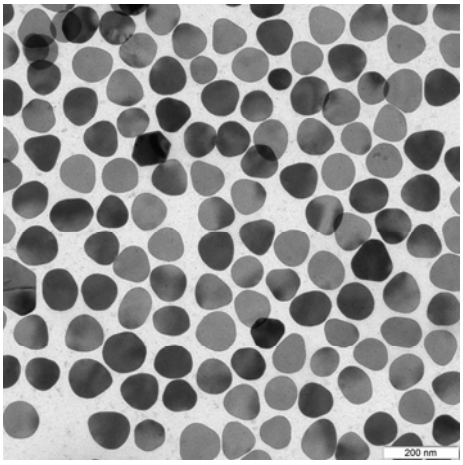

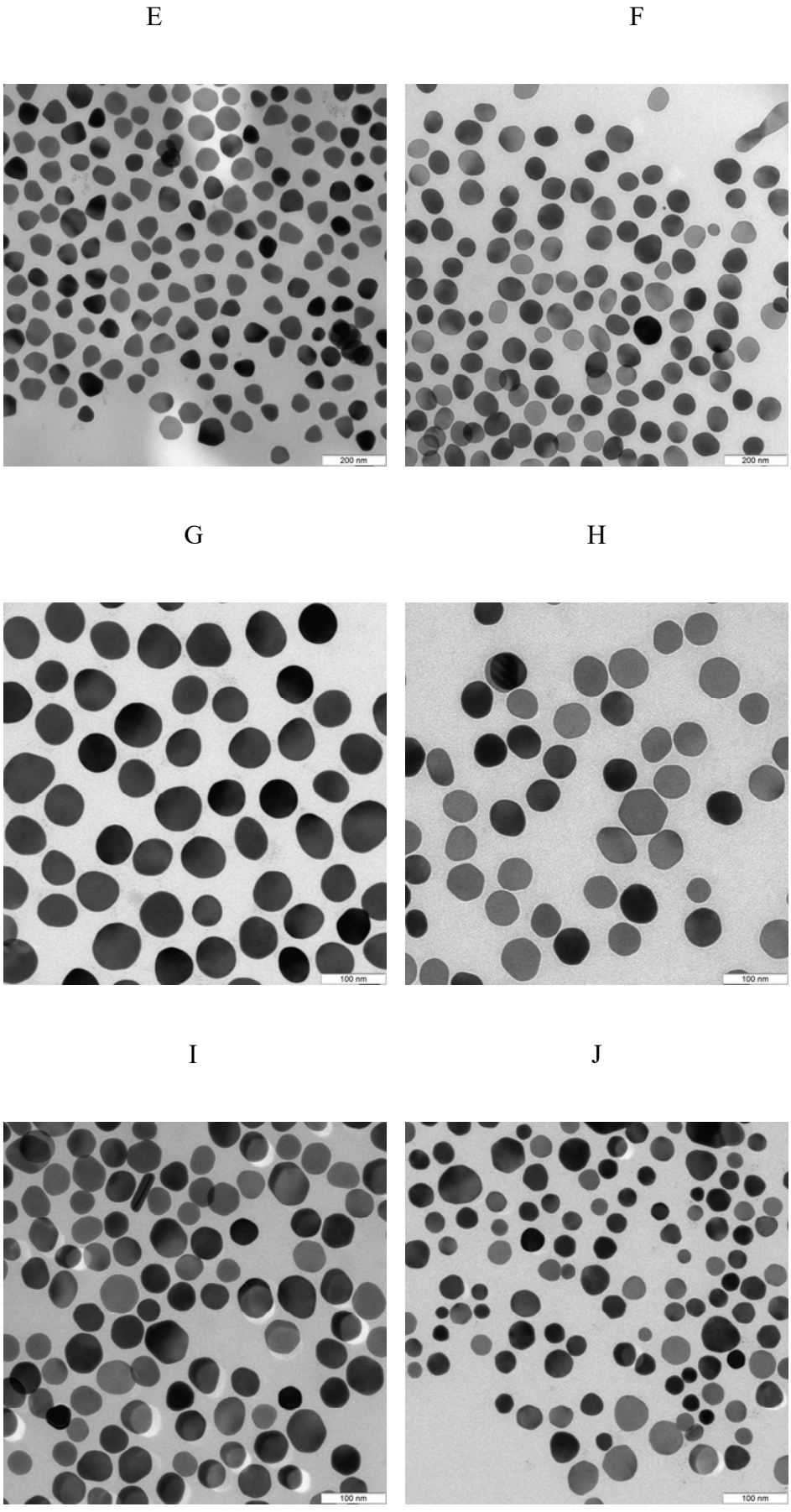

Figure S10. TEM images of AuNTs for the initial sample 0 (A, B) and etched samples 1-8 (C-J), respectively. The scale bars are 1 μm (A), 200 nm (B-F), and 100 nm (G-J)

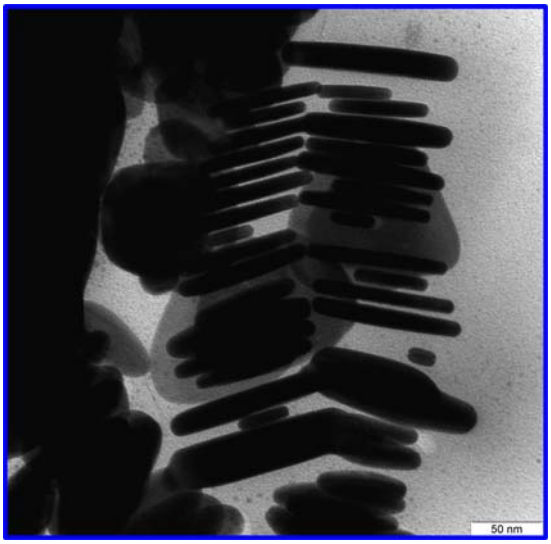

Figure S11. TEM image of AuNT stacks used for evaluation of AuNT thickness. The scale bar is 50 nm.

S2.2. A geometrical model to characterize the shape of initial AuNT particles

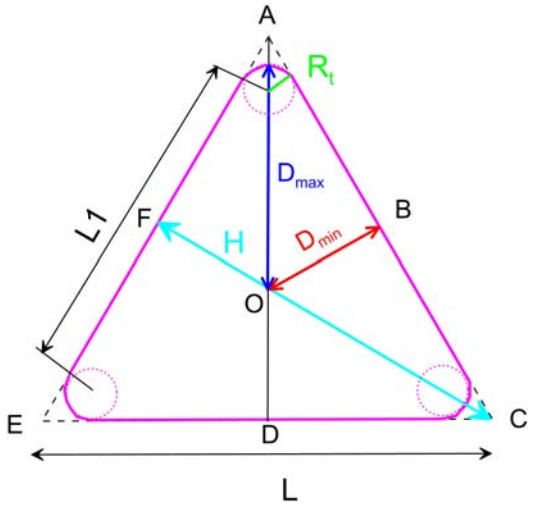

Figure S12. Two parameters $D_{\min}$ and $D_{\max}$ characterize the size and shape of Au nanotriangles. The other three parameters L, L_1, R_t can be expressed through $D_{\min}$ and $D_{\max}$, see below, Eqs (S1-S5).

From simple geometrical considerations, one can easily derive the following relations:

$$L = 2\sqrt{3}D_{\min}, \tag{S1}$$

$$L_1 = L - 2\sqrt{3}R_t, \tag{S2}$$

$$R_t = 2D_{\min} - D_{\max}, \tag{S3}$$

$$H = 3D_{\min}. \tag{S4}$$

Assuming the AuNT area to be equal to that of the triangle AEC, we get the surface equivalent diameter

$$D_{SE} = L\sqrt{\frac{\sqrt{3}}{\pi}} = 2D_{\min}\sqrt{3}\sqrt{\frac{\sqrt{3}}{\pi}} \simeq 2.57D_{\min}. \tag{S5}$$

To take into account the rounded triangle vertex, Eq. (S5) should be modified slightly

$$D_{SE}(\text{nm}) = 2.57D_{\min}(\text{nm}) - 3.5\text{nm}. \tag{S6}$$

In particular, for the AuNT sample 1, TEM analysis gives $D_{\min} = 43.4$ nm and $D_{SE} = 108.1$ nm. From Eq. (S5), we have almost the same value $D_{SE} = 108\,\text{nm}$.

Section S2.3. COMSOL simulation of extinction spectra for a fixed AuNT orientation and comparison with experiment.

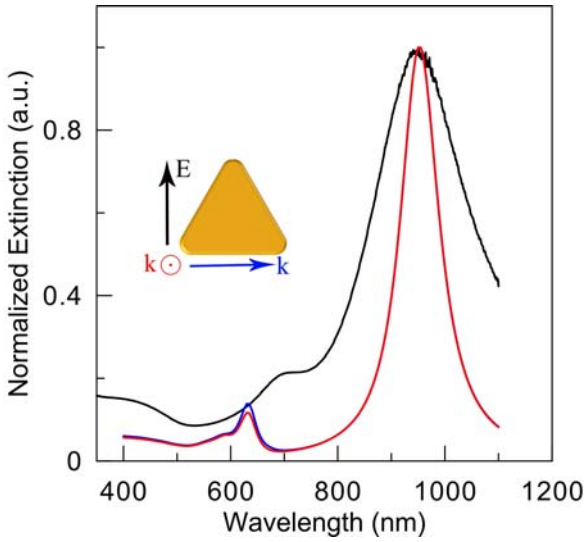

Figure S13. Comparison of experimental (black, the sample S1 with PR at 950 nm) and COMSOL-simulated (blue and red) extinction spectra. The simulations were performed for an AuNT model with the following parameters: $L = 160$ nm, $R_t = 15$ nm, thickness $t = 11$ nm, the incident field **E** lies in-plane, and the wave vector **k** lies in or out-of-plane. The dielectric function was taken from the bulk Johnson-Christy data. While the experimental and simulated major peak positions agree, the positions of multipole peaks differ by 70 nm. Note very close simulated spectra for in-plane and out-of-plane incidence.

Table S1. Extinction cross sections calculated at three resonance wavelengths for in-plane and out-of-plane incidence and in-plane excitation (Figure S13)

λ(nm)	C_{ext}(nm^2)		Difference (%)
	In-plane	Out-of-plane	
590	7904.7	7908.4	-0.05
635	14475.7	16545.5	-14.3
955	125163	119936	4.2

Section S2.4. SERS spectra for AuNT@NBT and AuNT@Cy7.5 samples at 785-nm laser excitation.

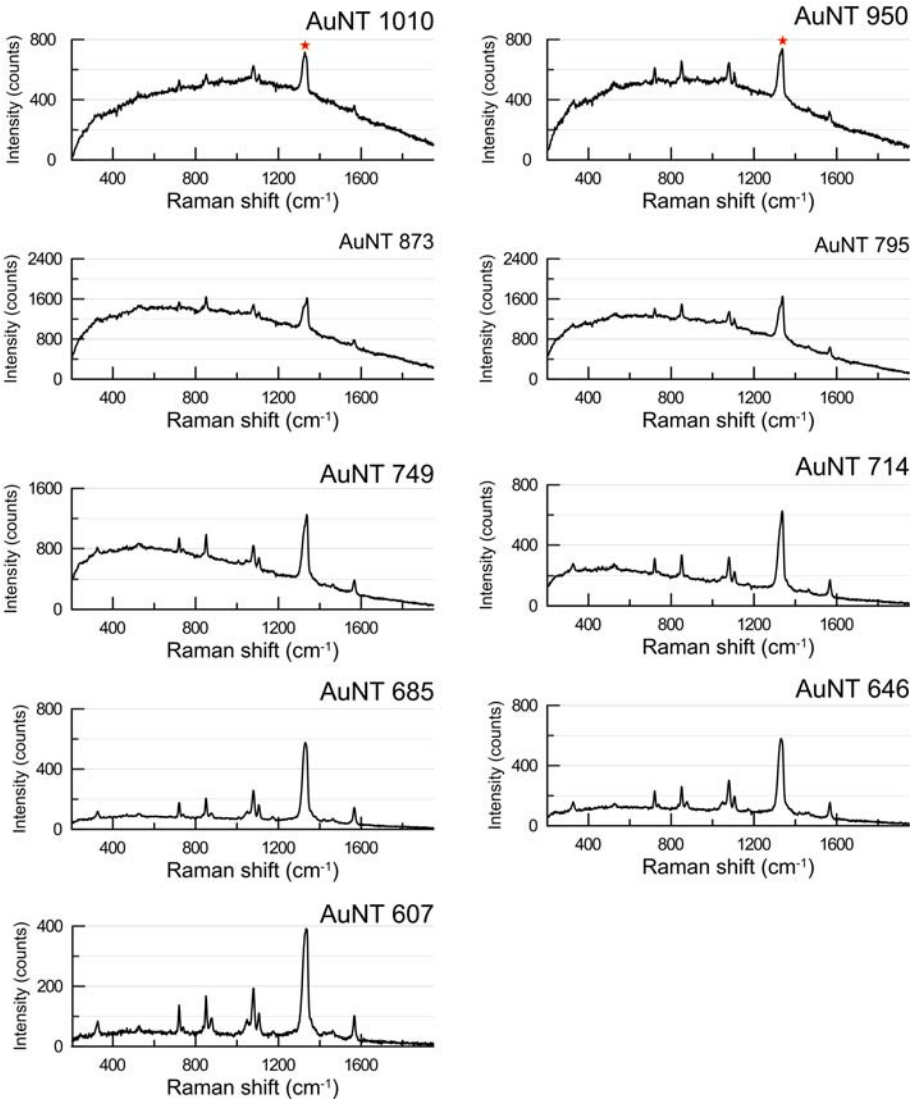

Figure S14. SERS spectra for AuNT@NBT samples measured at 785 nm laser excitation. The LPR wavelength decreases from 1010 to 607 nm.

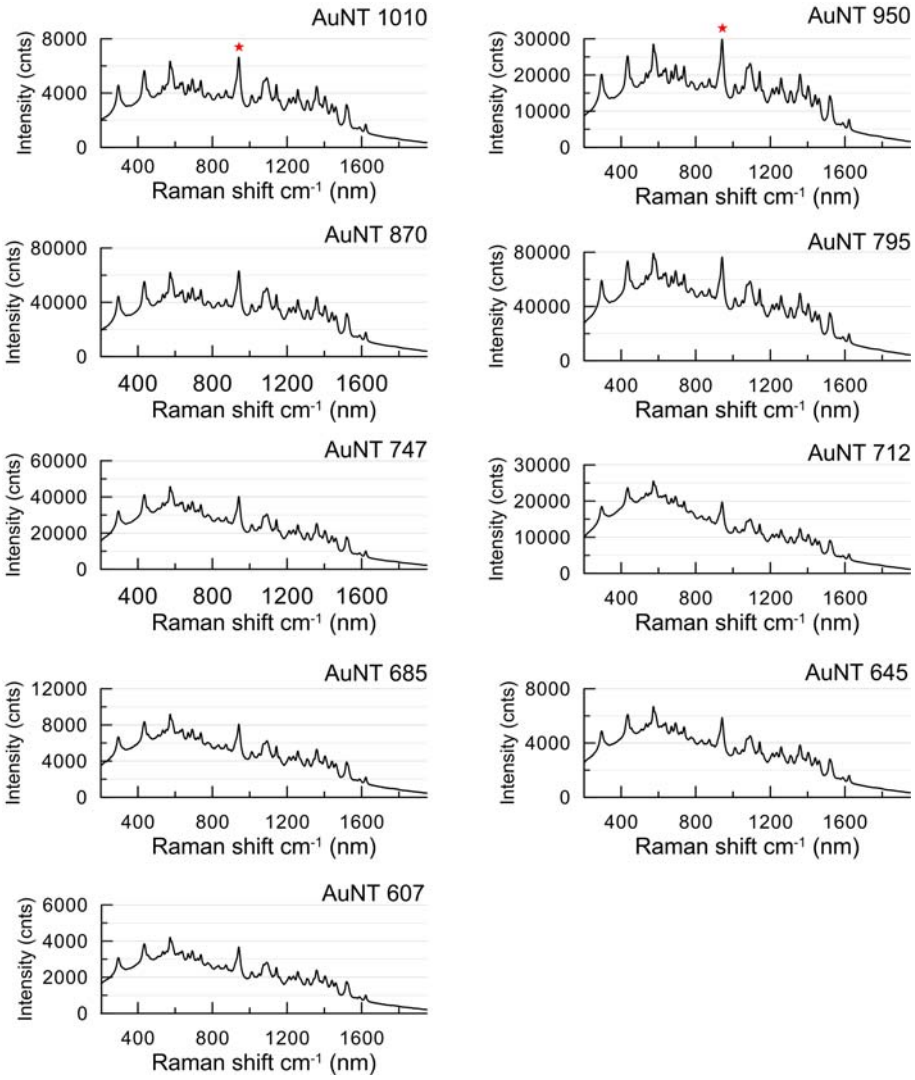

Figure S15. SERS spectra for AuNT@Cy7.5 samples measured at 785-nm laser excitation. The LPR wavelength decreases from 1010 to 607 nm.

Section S3. Calculations of the surface and orientation averaged SERS enhancement factor for AuNRs

Consider first the averaging of EF over the total outer AuNR surface S. By definition, $\langle EF \rangle_s$ equals[1]

$$\langle EF \rangle_s = \frac{1}{S}\int_S |E(\omega_L)|^2 |E(\omega_R)|^2 \, dS \,, \tag{S7}$$

where the squared modulus of fields are taken at the laser and Raman frequencies. Owing to the nanorod symmetry, it is sufficient to consider the upper half of the particle (Figure S16) and perform the averaging over the polar angles θ, ϑ.

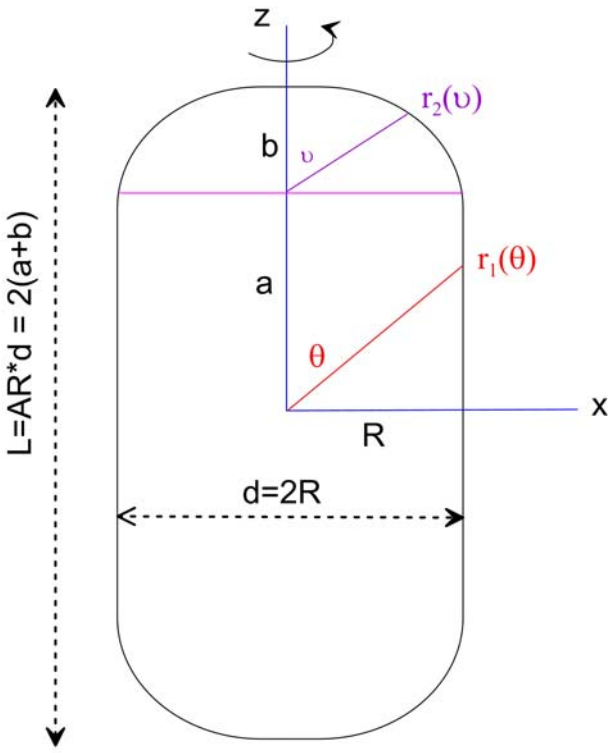

Figure S16. The geometry of a nanorod with the length L L, diameter of d, and elliptical caps with the cap height $b = \chi_c R$ and radius $R = d/2$. The radius vectors $r_1(\theta)$ and $r_2(\vartheta)$ describe the boundary shape.

It is convenient to consider the cylindrical part of the nanorod surface, S_1, and the cap surface S_2. The total surface averaged enhancement factor is

$$\langle EF \rangle = \frac{1}{S_1 + S_2}\left[EF_1 + EF_2\right] \tag{S8}$$

$$S_1 = 2\pi Ra = \pi R(L - 2b), \tag{S9}$$

$$S_2 = \pi Rb\left(q + \frac{\ln\left(q + \sqrt{q^2 - 1}\right)}{\sqrt{q^2 - 1}}\right), \tag{S10}$$

$$q = \frac{R}{b}. \tag{S11}$$

Equation (S10) gives a known expression for the surface area of an oblate spheroid with semiaxes b and $R \geq b$. If $R = b$, then the right part of Eq. (S10) in brackets equals 1 and $S_2 = 2\pi R^2$ equals the semisphere surface. In the opposite limit $b \to 0$, the expression with logarithm equals zero and $S_2 = \pi R^2$, as it should be.

The surface averaged enhancement factor $\langle EF \rangle_1$ can be calculated by averaging over the polar angle θ or, equivalently, over the cylindrical coordinate z

$$EF_1 = 2\pi R\int_0^a EF\left[r_1(z(\theta)\right]dz, \tag{S12}$$

$$r_1(z) = \sqrt{R^2 + z(\theta)^2}, \tag{S13}$$

$$z = R / \mathrm{tg}(\theta), \tag{S14}$$

$$\mathrm{tg}(\theta_{\min}) = \frac{R}{a}. \tag{S15}$$

Further, by using a general expression for any surface as given by rotation of an arbitrary curve $x = f(z)$ around the z-axis

$$S = 2\pi\int_0^b f(z)\sqrt{1 + [f'(z)]^2}\,dz, \tag{S16}$$

we get

$$EF_2 = 2\pi Rb\sqrt{q^2 - 1}\int_0^1 \sqrt{p^2 + t^2}\,EF\left(r_2(t)\right)dt, \tag{S17}$$

$$p^2 = \frac{b^2}{R^2 - b^2} = \frac{1}{(R/b)^2 - 1} = \frac{1}{q^2 - 1}, \tag{S18}$$

$$r_2(t) = \sqrt{R^2 - t^2(R^2 - b^2)}\,, \tag{S19}$$

$$z = bt, \quad x = R\sqrt{1-t^2}\,,\ r_2 = \sqrt{x^2 + z^2}\,. \tag{S20}$$

Equations (S20) relate the cap ellipse radius vector r_2 to the integration parameter t. If the enhancement factor in Eq. (S17) equals 1, then

$$\int_0^1 \sqrt{p^2 + t^2}\,dt = \frac{t\sqrt{p^2+t^2}}{2} + \frac{p^2}{2}\ln\left|t + \sqrt{p^2+t^2}\right|\Bigg|_0^1 = \frac{\sqrt{p^2+1}}{2} + \frac{p^2}{2}\ln\frac{1+\sqrt{p^2+1}}{p}, \tag{S21}$$

and we arrive at Eq. (S10) for the cap surface area.

The numerical evaluation of integrals (S12) and (S17) was carried out by using COMSOL codes:

Int_Snp(withsol('sol1',(up(ewfd.normE))^2/E0^2,setval(lambda0,wlL),setval(p,p))*withsol('sol1',(up(ewfd.normE))^2/E0^2,setval(lambda0,wlR),setval(p,p)))/Int_Snp(1).

Here, Int_Snp(1) is an operator of integration over the particle surface (it can be split by the sum of two integrals over the nanorod end and the cylindrical part; see Eq. S13); wlL and wlR are the laser and Raman wavelength, respectively. As we have two Raman lines, we used two analogous syntaxic procedures for wlR1 and wlR2). Finally, the expression ewfd.normE^2/E0^2 means the normalized squared modulus of the local field; the operator "up" points to the outer side. For details concerning other operators, the readers are referred to Refs.[2-4]

For orientation averaging, we used the following COMSOL options: "Data Series Operation —> Average" and "Method → Integration."

Section S4. Morphological parameters of AuNSTs.

Table S2. The average morphological parameters and LPR wavelengths of etched nanostars.

Sample	1	2	3	4	5	6	7	8
LPR (nm)	838	815	764	697	660	626	598	565
Tip length (nm)	25±4	22±4.8	21±4.5	16±4.5	13±4.6	12±4.3	13±3	9.9±2.7
Tip angle (degrees)	27±9.3	27±9.8	32±10	38±11	44±13	54±16	61±17	75±20
Core diameter (nm)	30±3.6	30±3.6	30±3.2	30±2.8	31±2.9	33±3.7	36±4.0	36±3.5

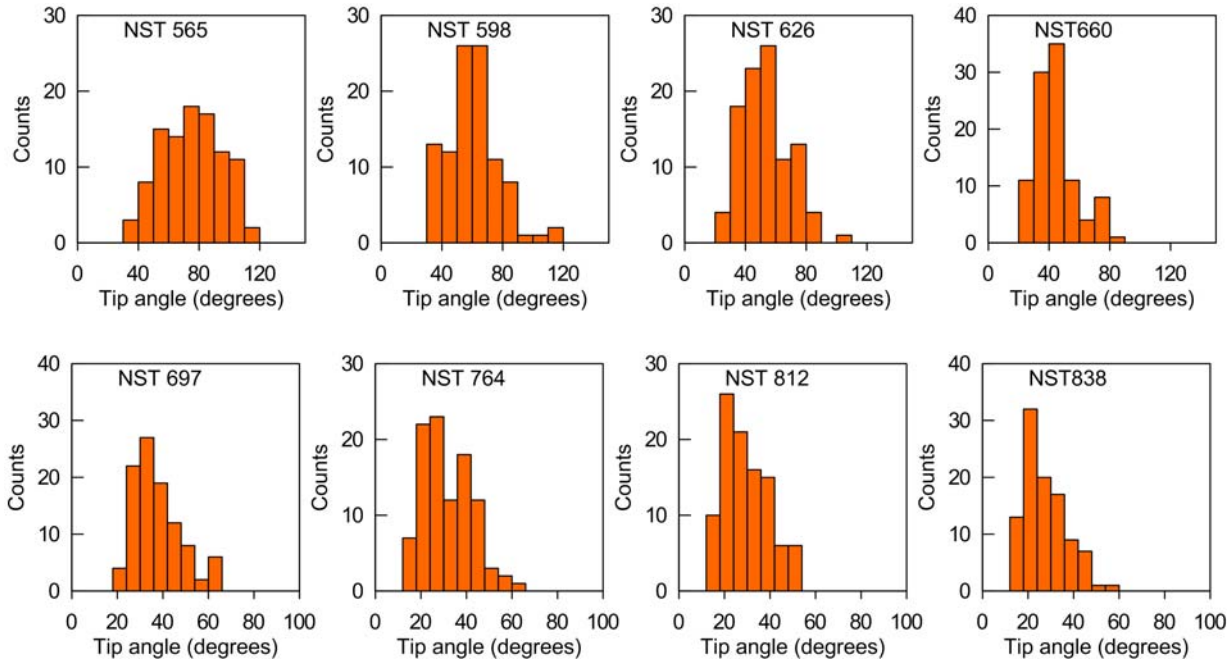

Figure S17. Histograms of the tip angle distributions for 8 samples NST 565-838.

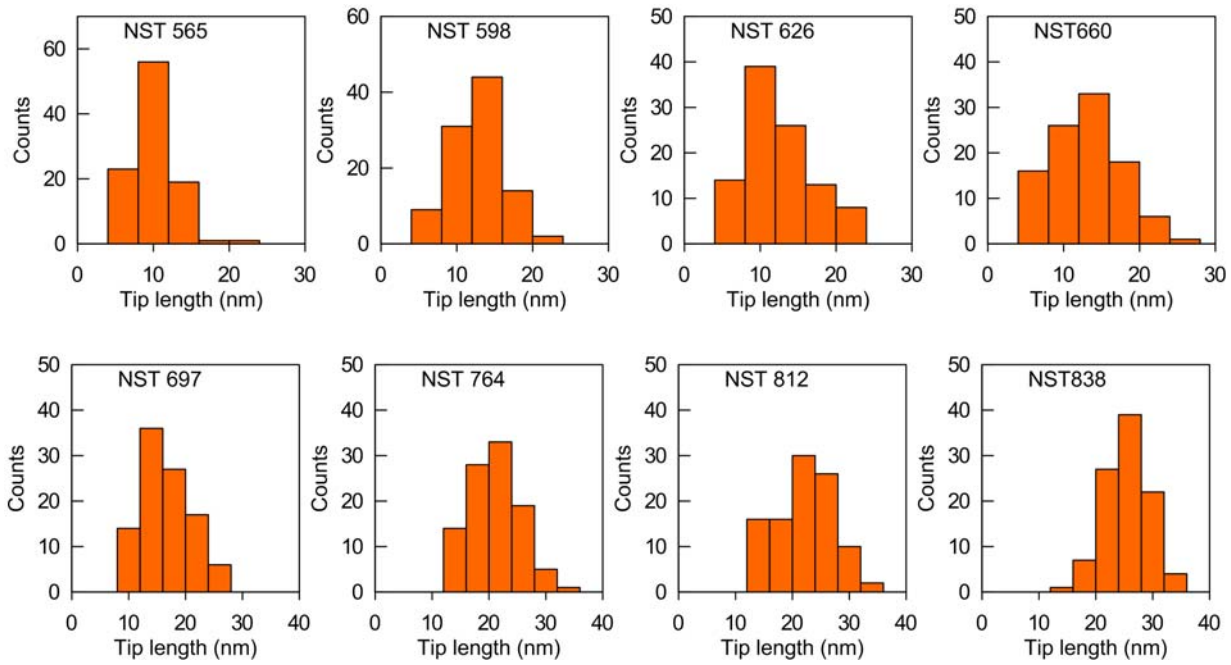

Figure S18. Histograms of the tip length distributions for 8 samples NST 565-838.

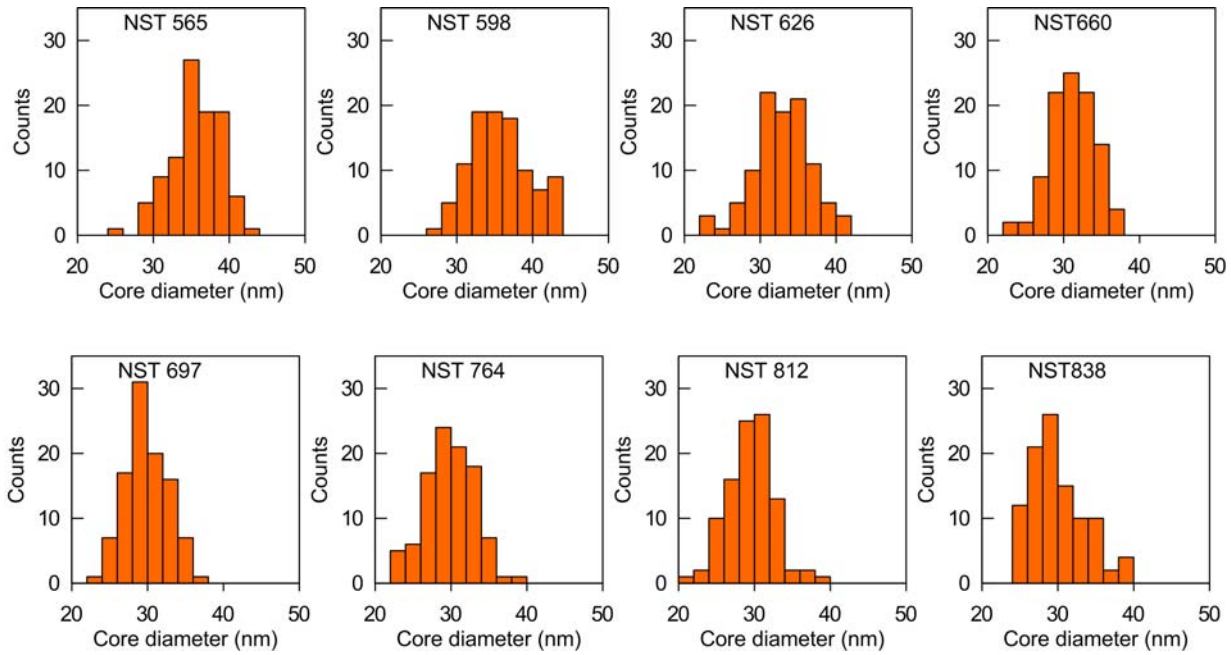

Figure S19. Histograms of the core diameter distributions for 8 samples NST 565-838.

Section S5. SERS spectra for AuNST@NBT and AuNST@Cy7.5 samples at 785 nm and 633-nm laser excitation

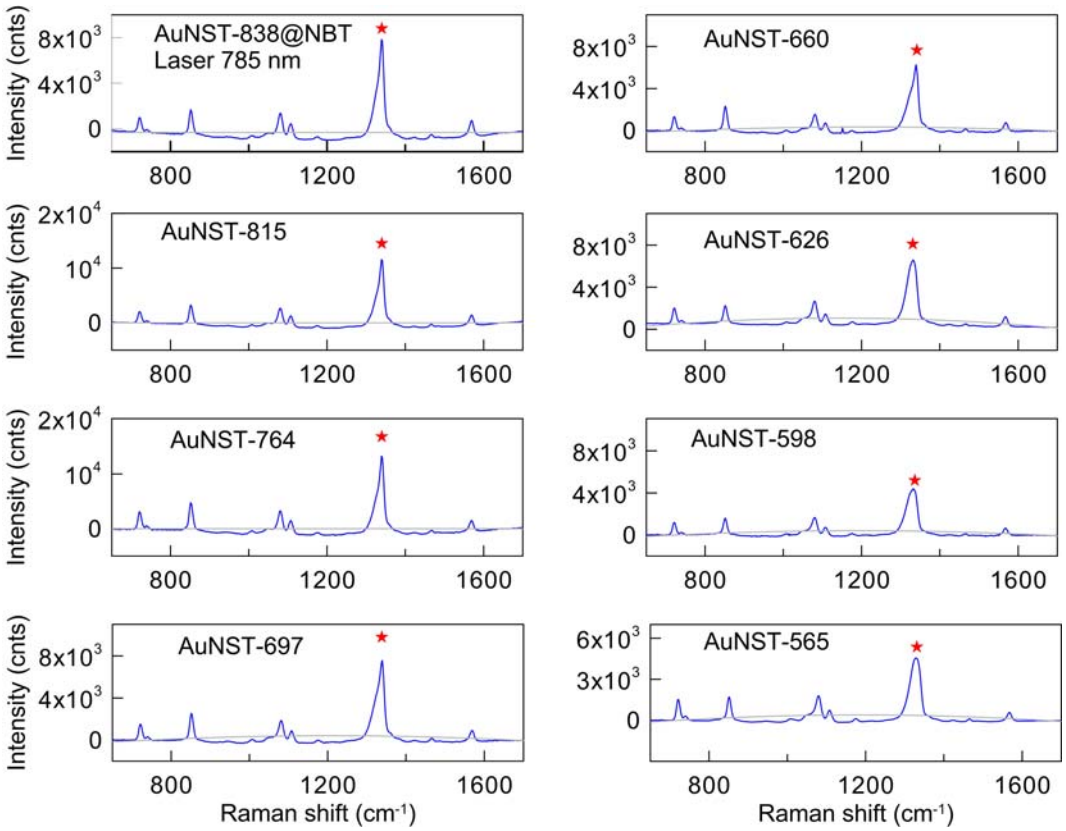

Figure S20. SERS spectra for AuNST@NBT samples measured at 785 nm laser excitation. The LPR wavelength decreases from 838 to 565 nm. The average fitted baseline (gray) was subtracted from the original spectra, thus explaining the negative values under the baseline.

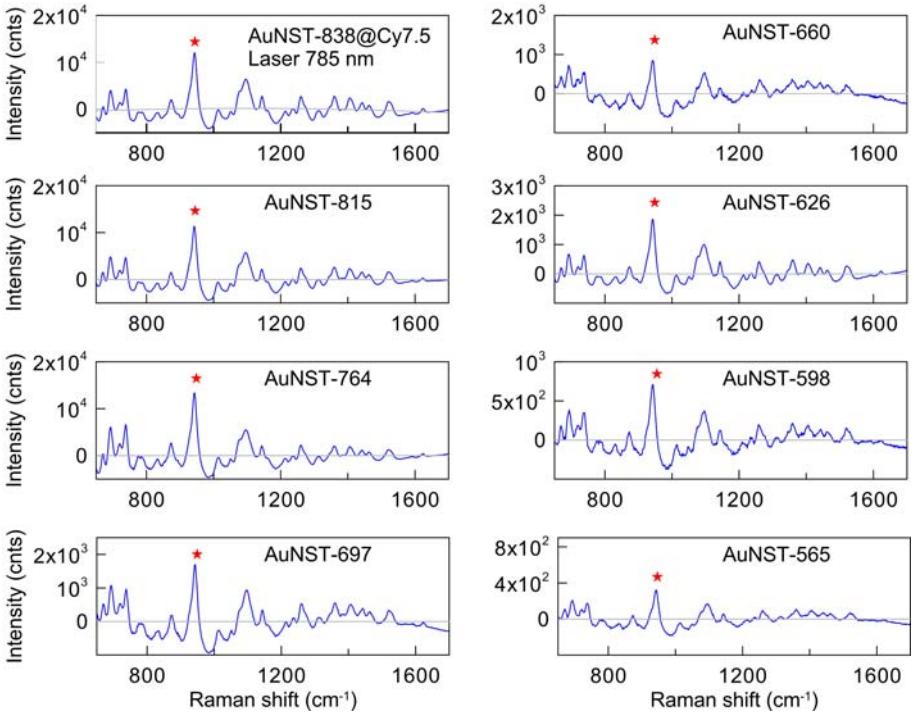

Figure S21. SERS spectra for AuNST@Cy7.5 samples measured at 785 nm laser excitation. The LPR wavelength decreases from 838 to 565 nm. The average fitted baseline (gray) was subtracted from the original spectra, thus explaining the negative values under the baseline.

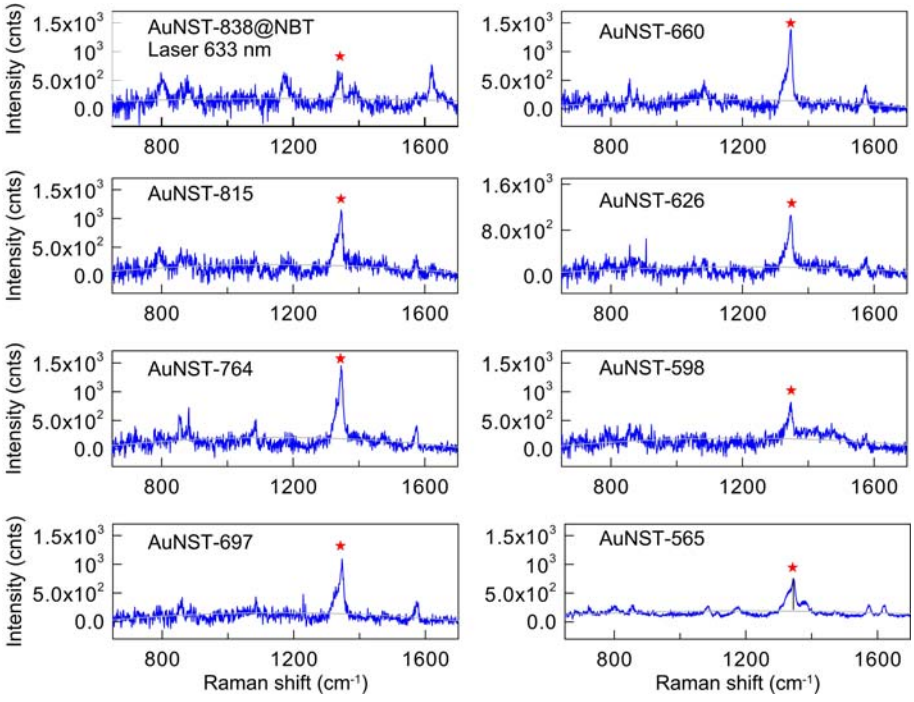

Figure S22. SERS spectra for AuNST@NBT samples measured at 633 nm laser excitation. The LPR wavelength decreases from 838 to 565 nm. The average fitted baseline (gray) was subtracted from the original spectra, thus explaining the negative values under the baseline.

References

(1) Khlebtsov, B. N.; Khanadeev, V. A.; Burov, A. M.; Le Ru, E. C.; Khlebtsov, N. G. Reexamination of Surface-Enhanced Raman Scattering from Gold Nanorods as a Function of Aspect Ratio and Shape. *J. Phys. Chem. C* **2020**, *124* (19), 10647–10658.

(2) URL:

https://www.comsol.com/support/learning-center/article/Examples-of-the-withsol-Operator-59801

(3) URL:

https://doc.comsol.com/6.1/doc/com.comsol.help.comsol/comsol_ref_results.36.025.html

(4) Grand, J.; Le Ru, E. C. Practical Implementation of Accurate Finite-Element Calculations for Electromagnetic Scattering by Nanoparticles. *Plasmonics* **2020**, *15*, 109–121.